

Infrared Spectra of Molecules in Disks with Gaps

Planets form in protostellar accretion disks

Laplace 1796

Shu et al 1993, PP III, 3

Evidence of disks around T Tauri stars

Mendoza 1968, ApJ, 151, 977

Shu, Adams & Lizano 1987, ARAA, 25, 23

Beckwith & Sargent 1996, Nature, 383, 139

Disks seen in silhouette with HST

McCaughrean & O'Dell 1996, AJ, 111, 1977

Evidence for planets from stellar motions

Marcy, Cochran & Mayor 1999, PP IV

Connection: can we find evidence of forming planets in disks?

Planet with $M > \text{Earth}$ will clear annulus in disk

Lin & Papaloizou 1993, PP III

Most direct way of observing: IR or sub-mm imaging of dust

Chandler & Richer 1999, Astrophysical Disks, 91

Lay, Carlstrom & Hills 1997, ApJ, 489, 917

Jayawardha et al. 1998, ApJ, 503, L79

Koerner et al. 1998, ApJ, 503, L83

to resolve a 1 AU wide annulus at 150 pc need 6 mas res

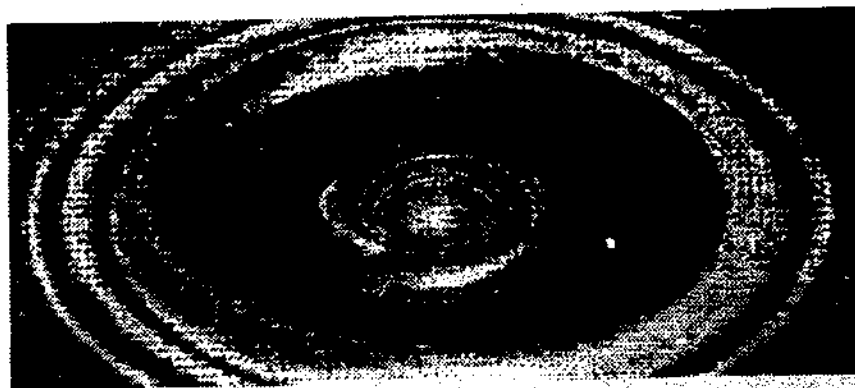


Figure 4. Surface density distribution for a gap opening protoplanet. A Jupiter mass protoplanet is initially embedded in a disc with $H/\alpha = 0.04$ and $\alpha_{vis} = 10^{-3}$ (α_{vis} refers to the standard viscosity parameterisation of Shakura & Sunyaev (1973)). The surface density near the planet (indicated by a white sphere) has been reduced by four orders of magnitude. Waves are clearly seen propagating both inward and outward away from the protoplanet.

HR 4796A

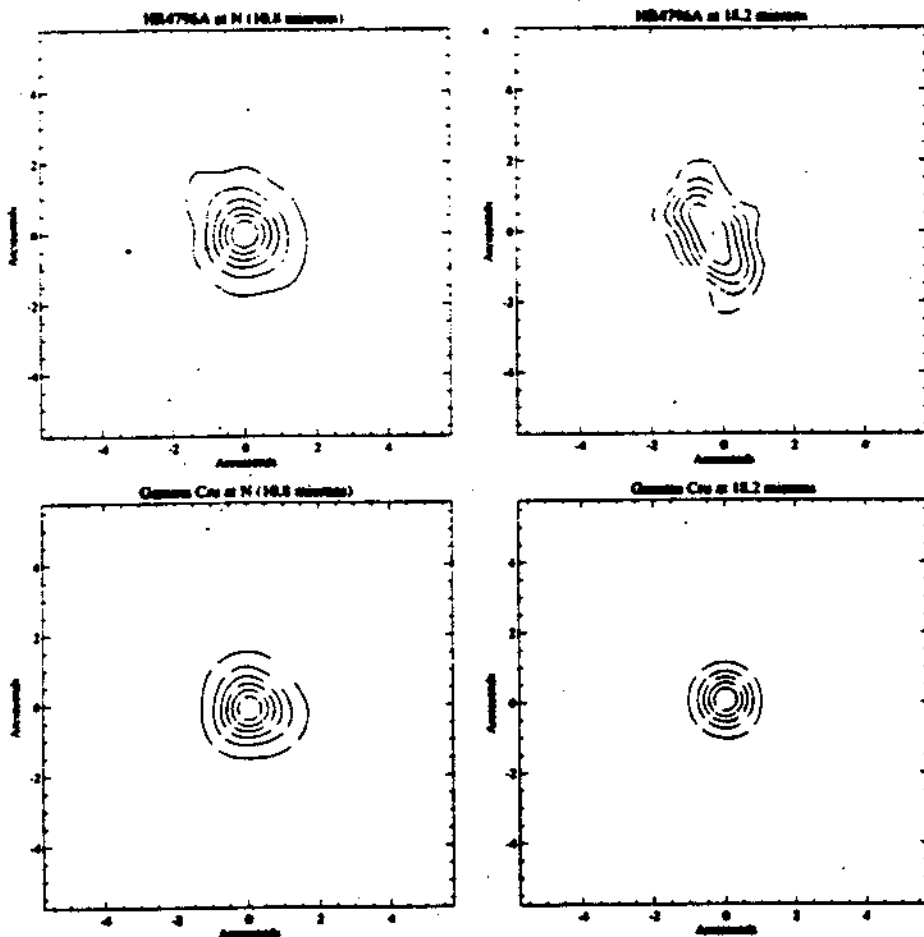


FIG. 2.—Surface brightness contour plots of the *N*-band (top left) and H1618 (top right) images of HR 4796A smoothed with a 5 pixel Gaussian. In the *N* image, the lowest contour is at $6.6 \text{ mJy arcsec}^{-2}$ and the contour interval is $9 \text{ mJy arcsec}^{-2}$. In the H1618 image, the lowest contour is at $44 \text{ mJy arcsec}^{-2}$ and the interval is $27 \text{ mJy arcsec}^{-2}$. In the bottom panels we show the corresponding PSFs, with contouring at the same fractional values of the peak emission as in the top panels. The lowest contour levels have been chosen to avoid the low-level, extended emission from the third diffraction ring in the PSF.

BOSS & YORKE

Vol. 469

ulations are
oints along
in opacities
(= gas) tem-
g v) from 1.3
inction are
l by Yorke
ins (silicates
ethane). For
in radius of
ensity to gas
 $\times 10^{12} \text{ g}^{-1}$,
the volatile
 10^{-5} cm , the
d the subli-
improve the
, a series of

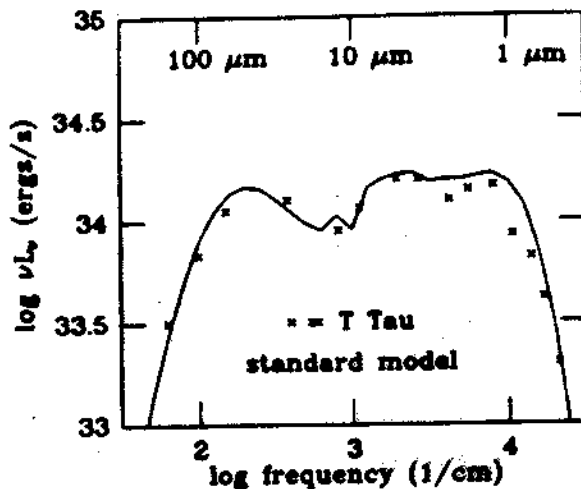


FIG. 1.—SED (solid line) for the standard model compared with nominal fluxes for T Tau (see text). The standard model is a protoplanetary disk with a mass of $0.02 M_{\odot}$ orbiting a solar-mass protostar, while undergoing mass accretion from an infalling envelope at a rate of $\sim 10^{-6}$ to $10^{-5} M_{\odot} \text{ yr}^{-1}$. Error bars for the nominal fluxes (not shown) are typically 1 to 2 times the height of the "cross" plot symbols (e.g., see Marsh & Mahoney's 1992 Fig. 1).

IN
ry disks with
e disk mass,

Less direct: effect of gap on SED

Mathieu, Adams & Latham 1991, AJ, 101, 2184

Beckwith 1999, PP IV

subtle because Planck function is so broad

grain emissivity, inclination, rad xfer can have > effect

Boss & Yorke 1996, ApJ, 469, 366

Better: effect of gap on Doppler profiles of molecular lines

still subtle - $v = v(r)$ but $z = z(v_{\text{los}})$

if matter is azimuthally symmetric, should be deconvolvable

MIR (vibrational) lines from planet-forming region (0.1-10 AU)

Carr & Najita 1997, Science with the NGST, 163

mm-wave (rot'n'l) lines are dominated by material > 100 AU

Sargent & Beckwith 1991, ApJ, 382, L31

Dutrey et al 1994, A&A, 309, 493

NIR lines are dominated by gas close to star

Najita et al 1999, PP IV

More difficult to observe than IR continuum

require $R \sim 100,000$ (3 km/s) $\sim 1/3 v(10 \text{ AU})$

Line strengths and shapes difficult to predict

L34

SARGENT & BECKWITH

Vol. 302

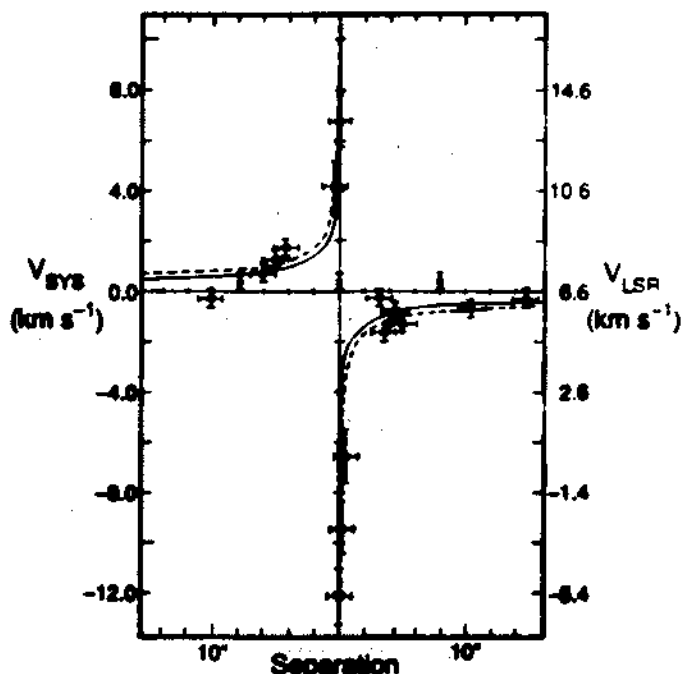


FIG. 3.—The observed rotation curve for HL Tau. Error bars indicate the uncertainties in position and velocity for the data points. The solid and dashed lines show the expected variation of peak position with velocity for material in Keplerian rotation about stars of mass 0.55 and $1 M_{\odot}$, respectively.

L32

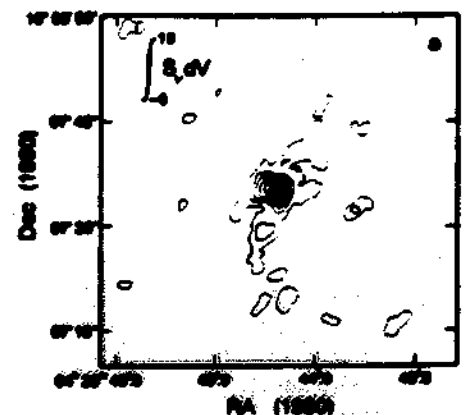


FIG. 1.—(a) A map of the ^{13}CO emission around HL Tau at 30%, 40%, 50%, 60%, 70%, and 90% of the peak flux, 7.3 Jy beam^{-1} km s^{-1} , integrated over the velocity range $4.6\text{--}6.2 \text{ km s}^{-1}$. Contours begin the position of peak emission, $2.0 \text{ Jy beam}^{-1} \text{ km s}^{-1}$, again over velocity range $4.6\text{--}6.6 \text{ km s}^{-1}$. Contours begin at the 3σ level, 15

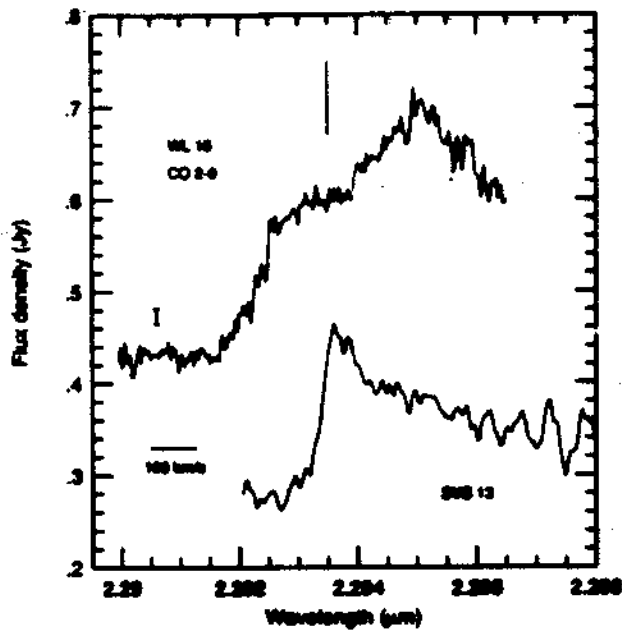


FIG. 1.—Spectrum of the $v = 2-0$ CO bandhead in WL 16, with a velocity resolution of about 13 km s^{-1} . The spectrum has been rotated with a standard star. The vertical line marks the rest wavelength of the bandhead. The error bar shows the 1σ noise in the WL 16 spectrum. Shown for comparison is the spectrum of SY 13 (plotted on an arbitrary scale), a young stellar object with a narrow CO velocity dispersion.

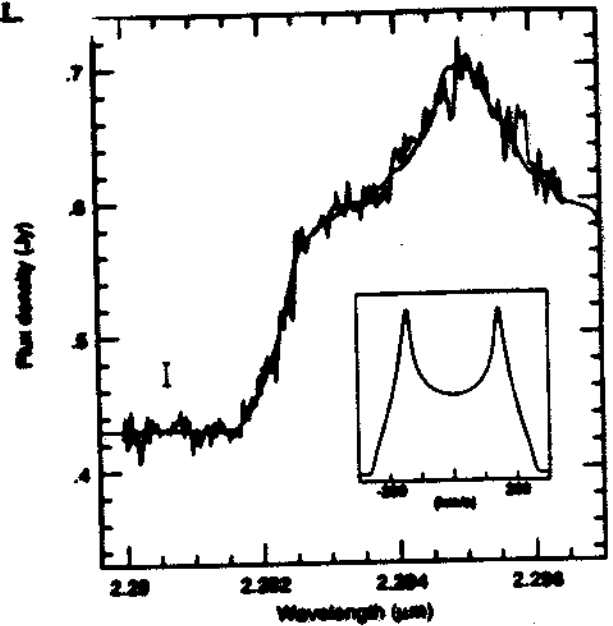


FIG. 2.—WL 16 spectrum overlaid with the best-fit model disk profile (smooth line). The model parameters are $V \sin i = 140 \text{ km s}^{-1}$, $\beta = 3.33$, $\alpha = 1.5$, and a LSR radial velocity of $+12 \text{ km s}^{-1}$. The figure inset shows the line profile as it would appear for a single emission line (not to scale).

Carr & Najita

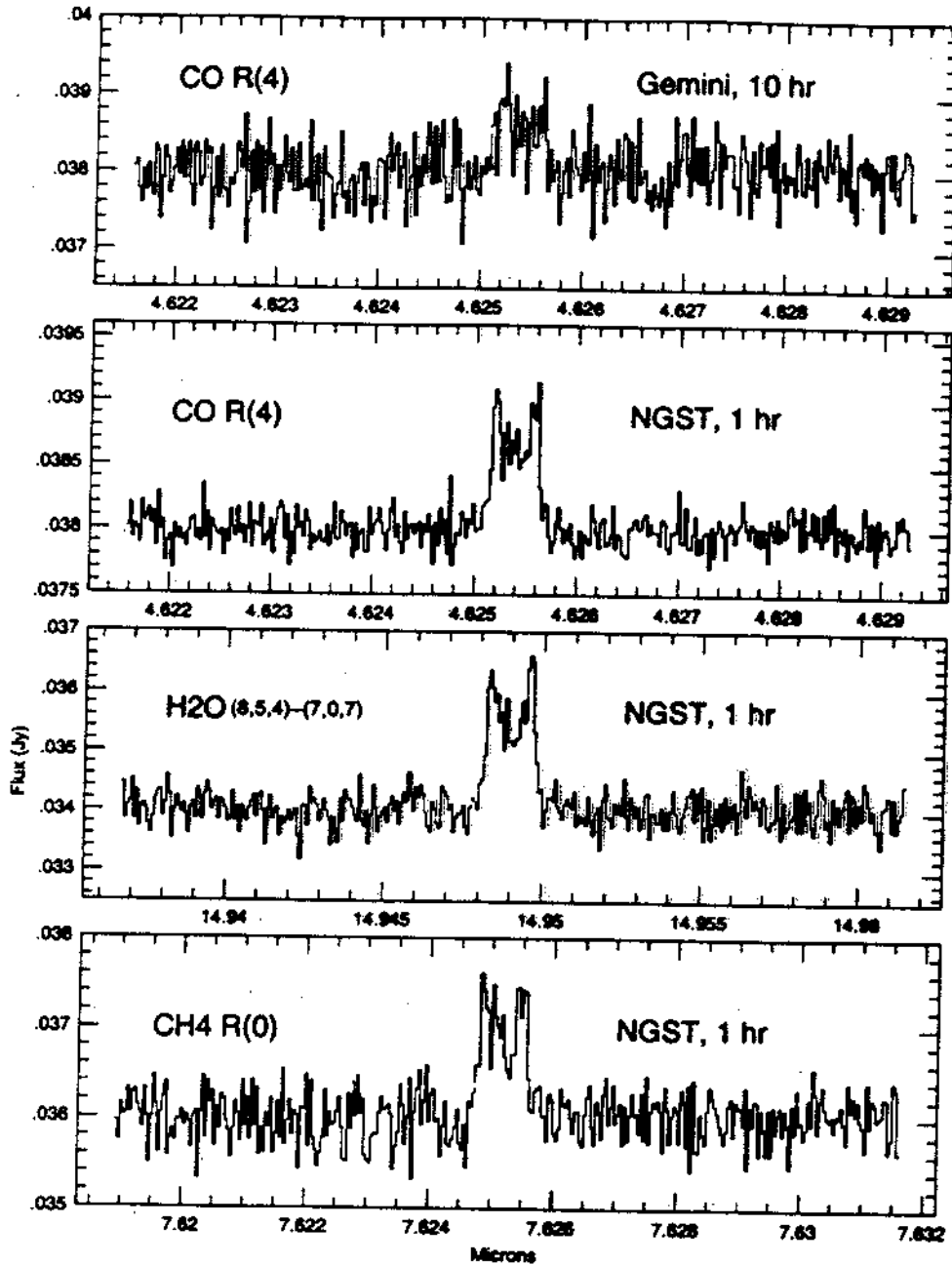
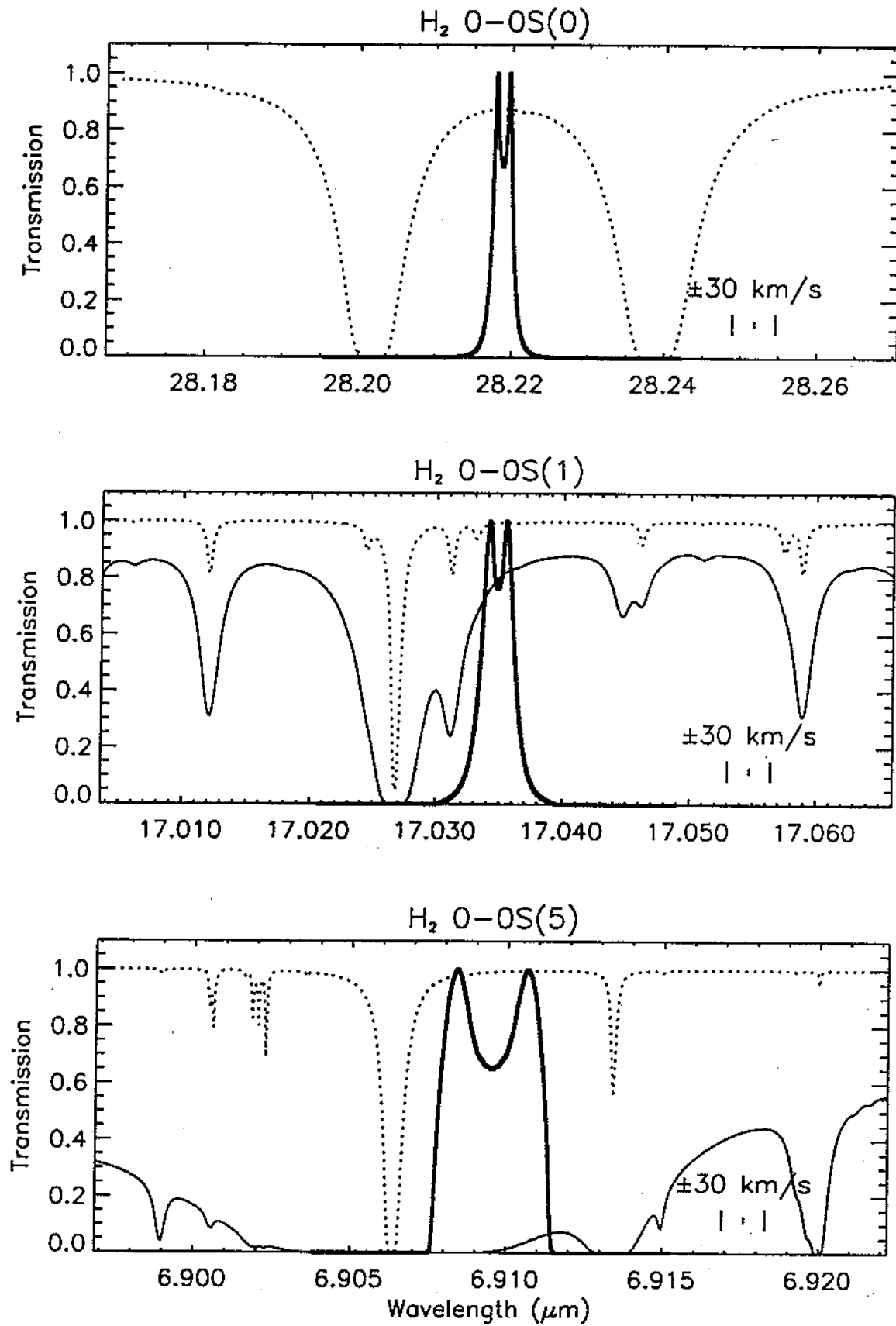


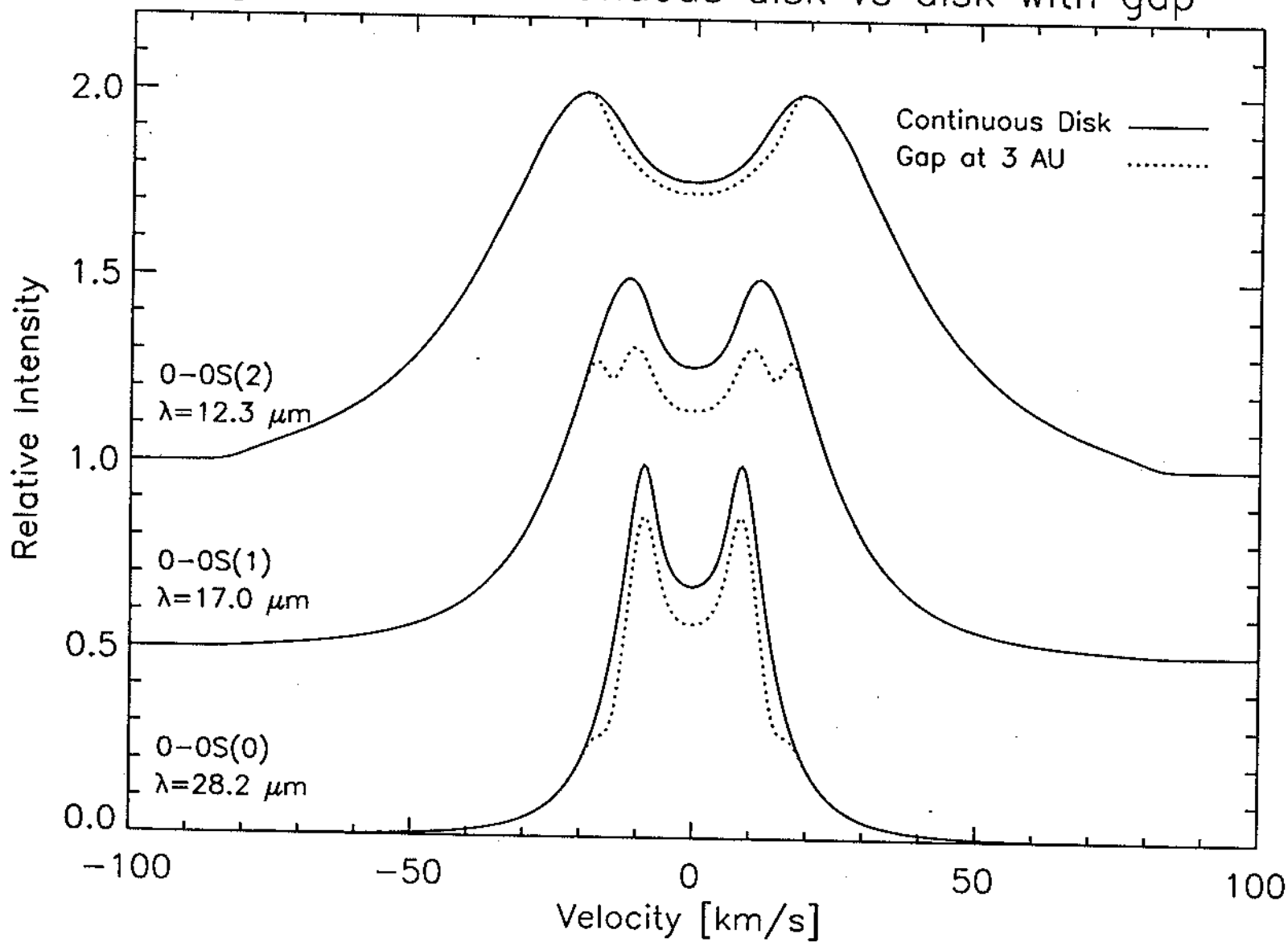
Figure 3. Simulated molecular line emission ($R=100,000$) from a disk gap created by the formation of a $1 M_J$ planet at an orbital radius of 1 AU from a T Tauri star at the distance of Orion. *Top panel:* CO ($v=1-0$) emission, as observed by Gemini in 10hr. *Lower 3 panels:* Lines of CO, H₂O, and CH₄, as observed by a thermal IR spectrograph on NGST. The gain in speed over ground-based spectrographs is evident. The H₂O and CH₄ lines fall in highly absorbed regions of the atmosphere are not observable from the ground.

Richter

SOFIA and Mauna Kea Atmospheric Transmission



H₂ Profiles in continuous disk vs disk with gap



Richter

Theory needed to calculate line profiles

$\rho_g(r,h)$, $\rho_d(r,h)$

flat or flared

Kenyon & Hartmann 1987, ApJ, 323, 714 Bell poster

Chiang & Goldreich 1997, ApJ, 490, 368

changes caused by planets

Papaloizou, Terquem & Nelson 1999, Ap Disks, 186

Lin, Bryden & Ida 1999, Astrophysical Disks, 207

Takeuchi, Miyama & Lin 1996, ApJ, 460, 832

$T_g(r,h)$, $T_d(r,h)$

heating - accretion vs. starlight active vs. passive

Shakura & Sunyaev 1973, A&A, 24, 337

Lynden-Bell & Pringle 1974, MNRAS, 168, 603

Adams, Lada & Shu 1987, ApJ, 312, 788

Adams, Ruden & Shu 1989, ApJ, 347, 959

coupling of gas and dust

cooling

Molecular abundances

Prinn 1993, PP III, 1005

Willacy et al. 1989, A&A, 338, 995

Aikawa et al. 1997, ApJ, 486, L51

Molecular excitation + radiative transfer

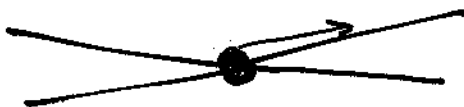
Details for specific objects

inclination

Chiang & Goldreich 1999, preprint

reddening

wind + envelope contribution



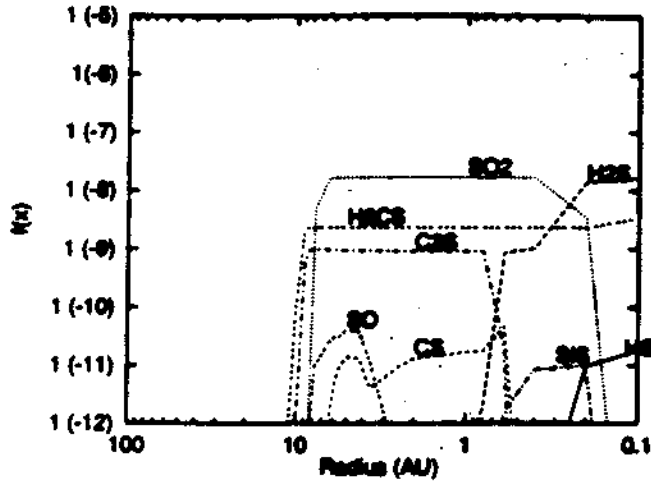


Fig. 3. The radial distribution of the fractional abundances (with respect to the total density) of sulphur bearing molecules in the CRH model. The destruction of SO_2 at small radii is due to collisional dissociation and leads to the formation of H_2CS , HS and SiS .

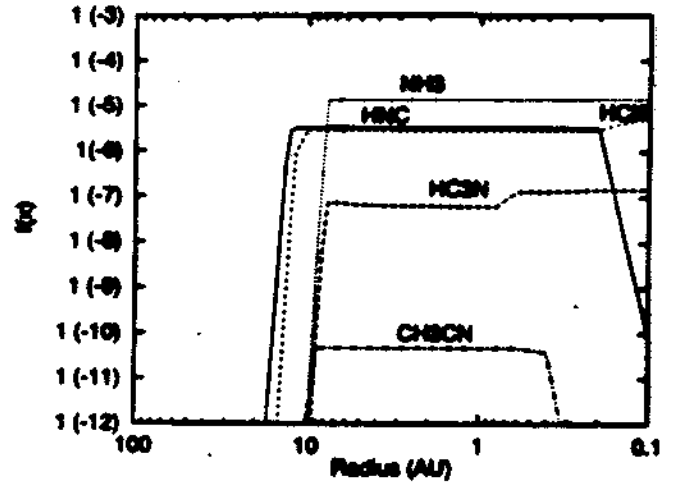


Fig. 5. The fractional abundances with respect to the total hydrogen abundance of the nitrogen-bearing molecules.

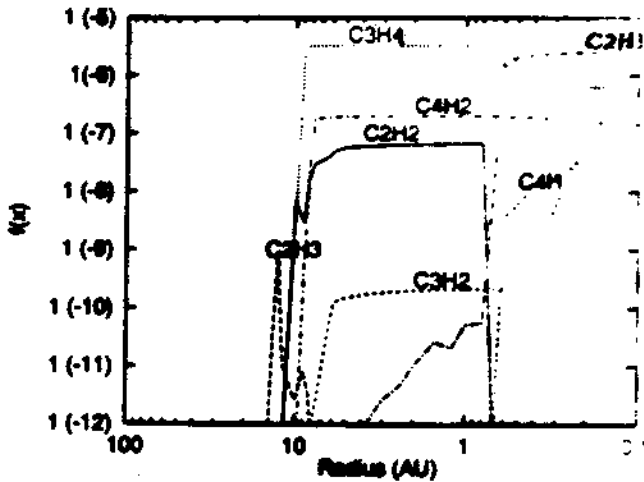


Fig. 4. The radial distribution of the carbon chain molecules with respect to the total density in the CRH model.

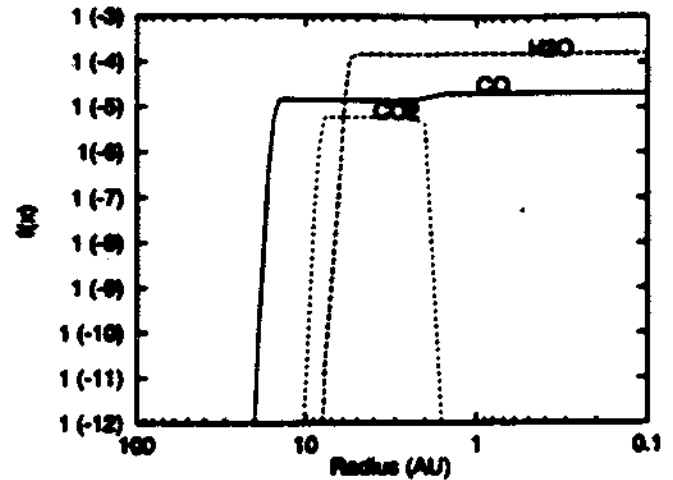


Fig. 2. The variation in the fractional abundance with respect to the total density of CO , CO_2 and H_2O with radius in the CRH model. The reappearance of the molecules in the gas is due to thermal desorption and the difference in the binding energies of the molecules is reflected in the different radii at which this occurs. CO_2 is destroyed at 2 AU by reaction with H_2 .

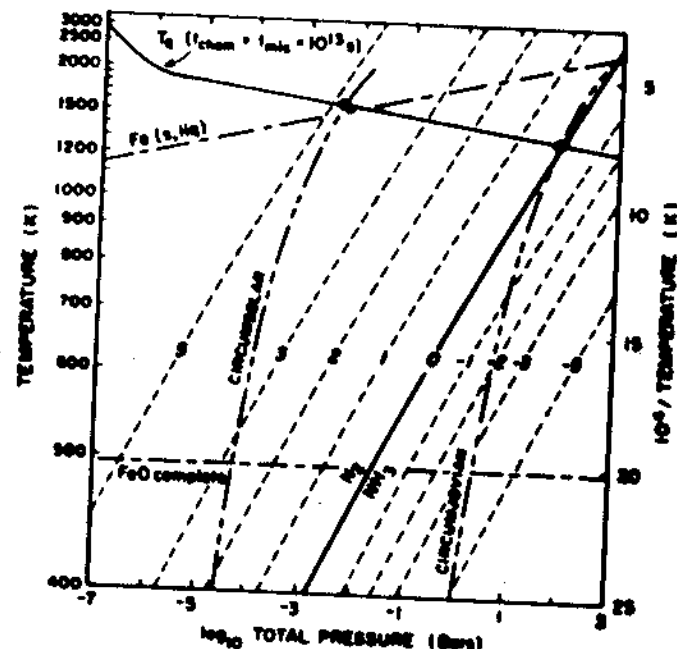
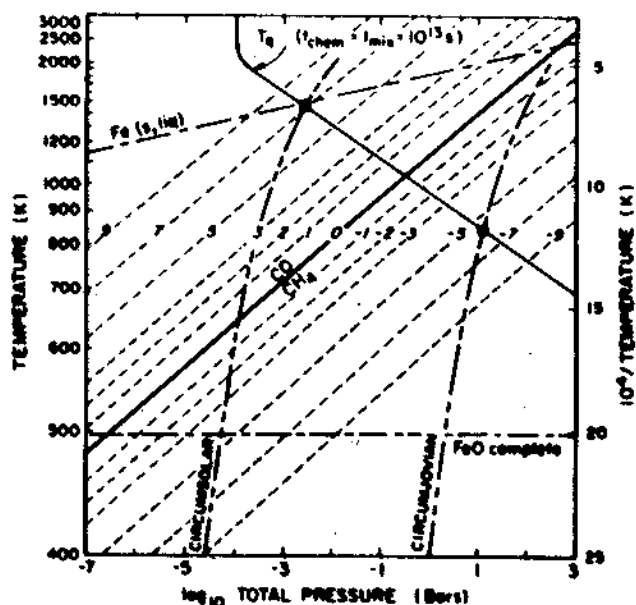


Figure 1. Thermochemical equilibrium $\log_{10}(\text{CO}/\text{CH}_4)$ values in a solar composition medium with $[\text{C}/\text{O}] = 0.6$. Also shown are illustrative temperature-pressure profiles for the circumsolar and circumjovian disks and the quench temperature T_q for homogeneous (gas-phase) conversion of CO to CH_4 assuming an upper limit for $t_{\text{mix}} = 10^{13}$ s. Heterogeneous (iron-catalyzed) conversion is possible between the lines designating the iron condensation temperature labeled "Fe(s,liq)" and the temperature where oxidation of Fe to FeO is complete, labeled "FeO complete."

Figure 2. As in Fig. 1 but for the $[\text{N}_2]/[\text{NH}_3]$ ratio and conversion of N_2 to NH_3 .

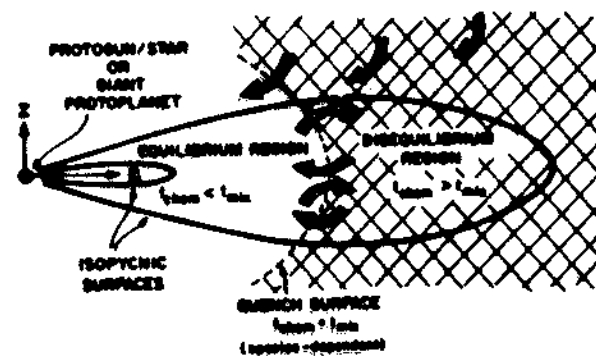


Figure 5. Illustration of the species-dependent quench surface separating thermochemical equilibrium and transport-induced disequilibrium regions in gaseous circumsolar or circumjovian planetary disks.

Existing Observations

CO overtone bandhead

Carr et al 1993, ApJ, 411, L37

Chandler et al 1993, ApJ, 412, L71

CO fundamental lines

Carr & Najita 1997, Science with the NGST, 163

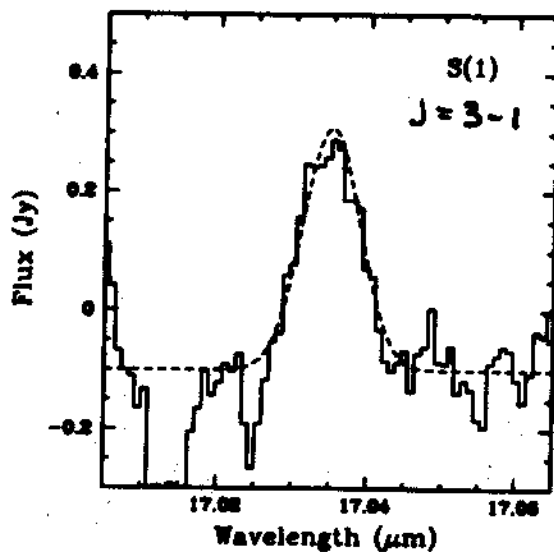
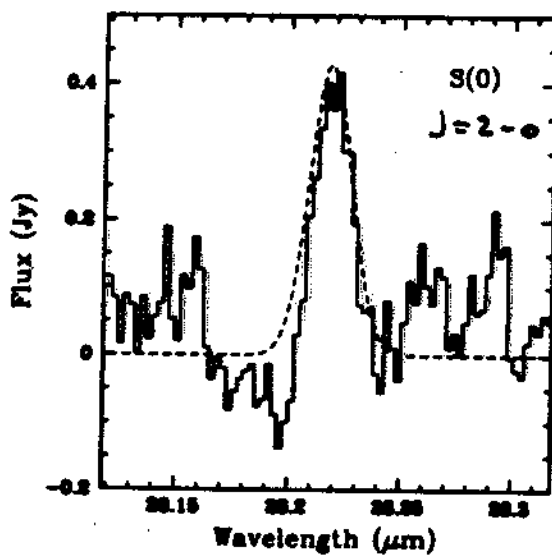
Najita et al 1999 pp IV

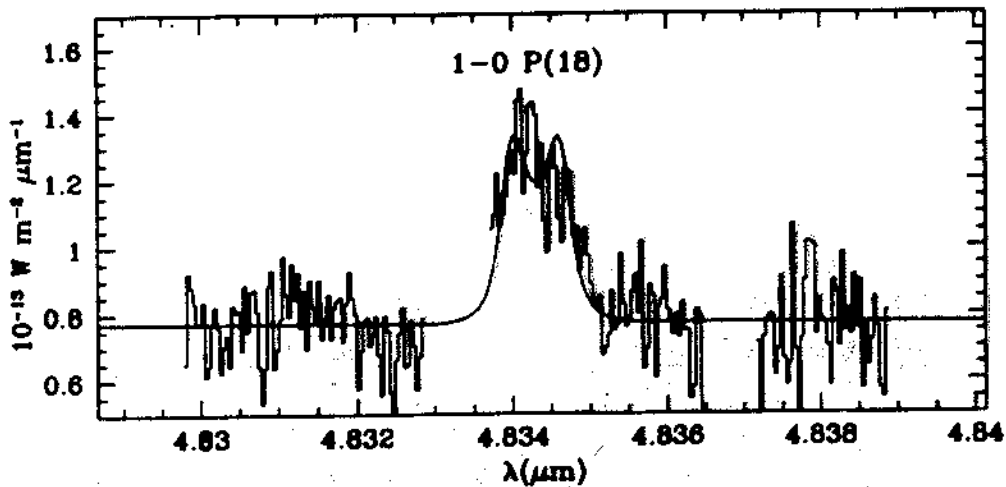
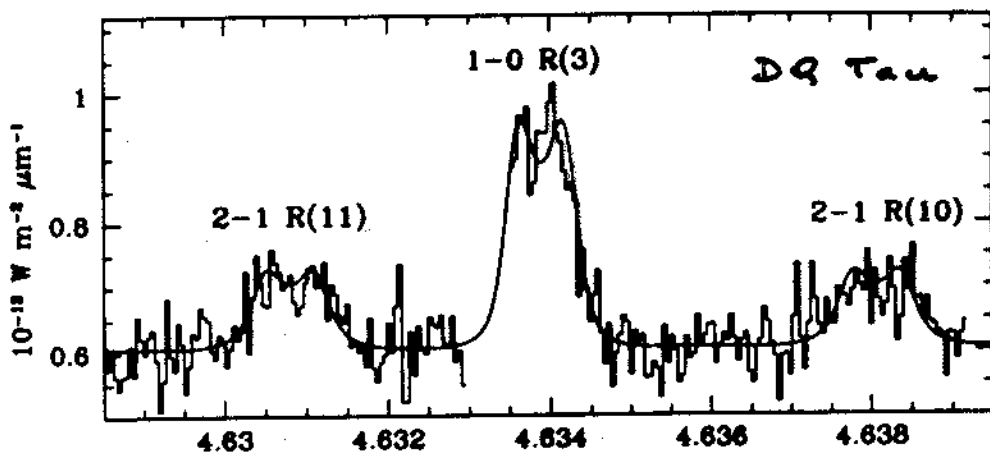
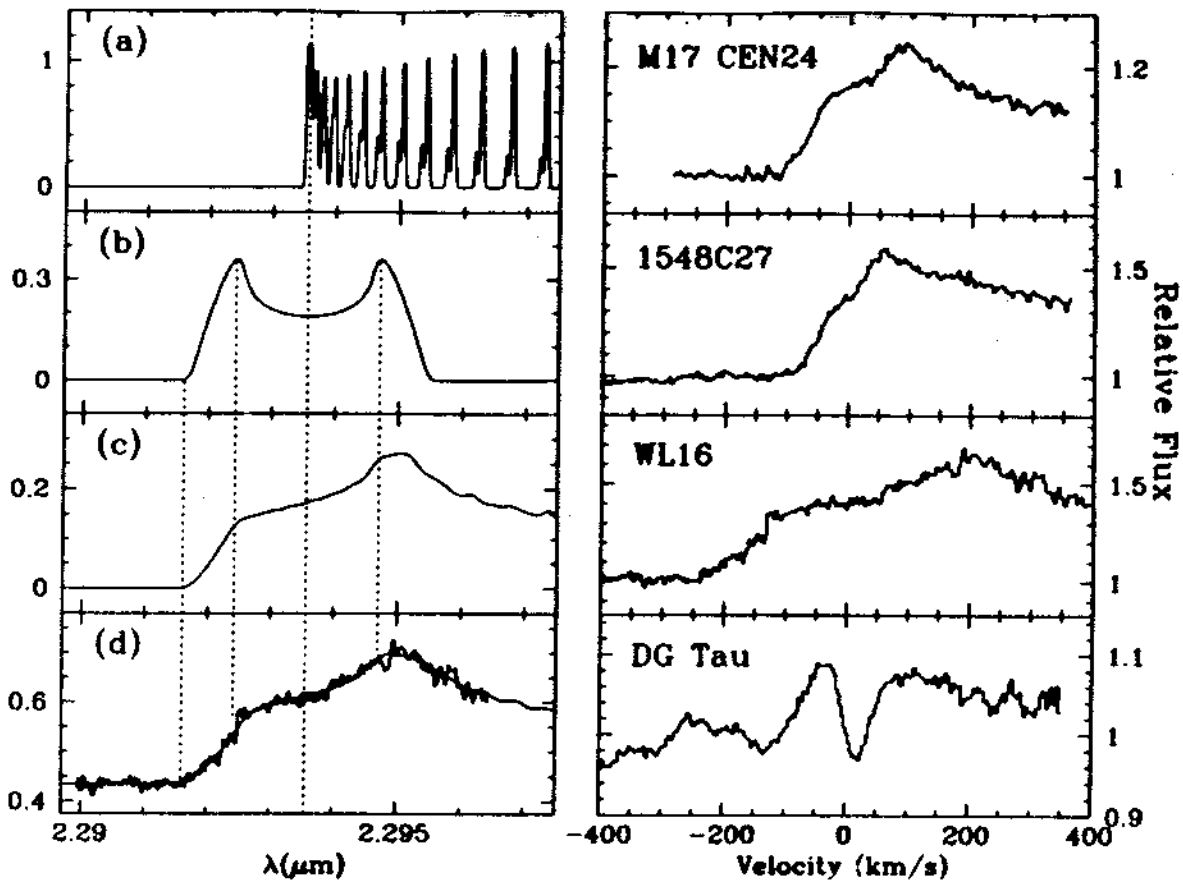
H₂

van Dishoeck et al 1998, Ap&SS, 255, 77

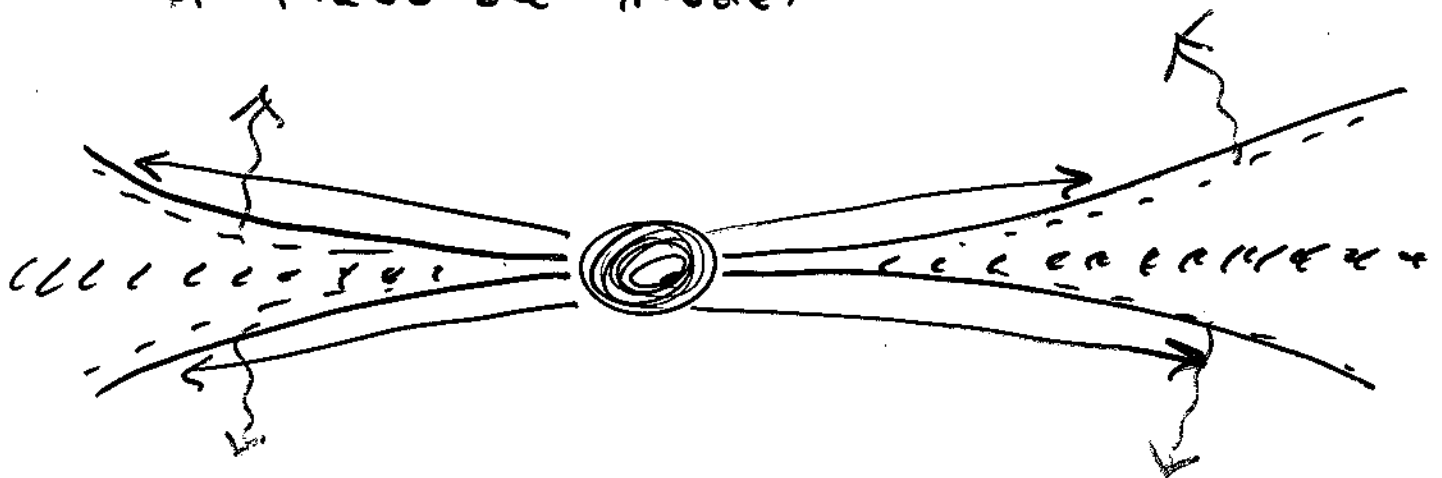
Thi et al 1999, preprint

λ : et al.





A Plausible Model



Chiang + Goldreich

surface layer:

$$T_d \approx 550 \text{ K } a_{\text{AU}}^{-2/5}$$

$$T_g \leq T_d$$

$$n_g \approx 10^8 \text{ cm}^{-3} a_{\text{AU}}^{-1}$$

interior
 $T_g = T_d \approx 150 \text{ K } a_{\text{AU}}^{-1/2}$
depends on dust settling

In MIR hot dust dominates continuum
 \Rightarrow dilute black body

If large grains settle by 1000

$$\tau_{\text{H}_2} > \tau_d \quad \text{in hot layer}$$

$$\Rightarrow \text{H}_2 \quad J=2-0, 3-1 \quad \text{in emission}$$

Other molecules not in vib'l LTE

\Rightarrow in absorption in MIR?

Observations with SOFIA

EXES (w/ Richter, Jaffe, Greathouse)

cross-dispersed mid-infrared
(5-28 μm) spectrograph

$R > 100,000$ at $\lambda < 10 \mu\text{m}$ (3 km s^{-1})

$\Delta v < 0.01 \text{ cm}^{-1}$ at $\lambda > 10 \mu\text{m}$ ($0.3 \lambda \text{ km s}^{-1}$)

photon noise $1/d \Rightarrow$ NEFD $\sim 5 \text{ Jy}$ at $7 \mu\text{m}$
 $\sim 20 \text{ Jy}$ at $20 \mu\text{m}$

NELB $\sim 2 \times 10^{-7} \text{ W/m}^2 \text{ sr}$
(15 in 15)

AIRES (Haas, Erickson, et al)

similar resolution, sensitivity for $\lambda > 17 \mu\text{m}$

GG Tau H_2 $J=2-0, 3-1$

$\sim 0.3 \text{ Jy}$ at $R \sim 2000$

if compact, $\sim 15 \text{ km s}^{-1}$ wide : 3 Jy

\Rightarrow S/N ~ 1 in 1 min.

[assuming 80% EE in 2" dia]

Mid-Infrared Molecular Bands

H_2 : $J=2-0$ ($28\mu m$), $3-1$ ($17\mu m$) ... $11-9$ ($5\mu m$)

CH_4 : ν_4 ($7.6\mu m$)

H_2O : ν_2 ($6\mu m$) hi-J rot'nd ($\sim 20\mu m$)

NH_3 : ν_2 ($10\mu m$)

CO : $\nu=1-0$ ($5\mu m$)

SiO : $\nu=1-0$ ($8\mu m$)

C_2H_2 , HCN : ν_5 , ν_2 ($13-14\mu m$)

CN , HNC , HCO^+ , OCS , S_2

Other Observatories

TEXES on IRTF

NEFD \approx SOFIA

on Keck

NEFD \approx SOFIA/1.0

NGST w/ $R=100,000$

NEFD \approx SOFIA/1000